Fundamental Analyses of 60 GHz Human Blockage

Martin Jacob, Sebastian Priebe
and Thomas Kürner
Technische Universität Braunschweig
Braunschweig, Germany
jacob@ifn.ing.tu-bs.de

Michael Peter, Mike Wisotzki,
Robert Felbecker and Wilhelm Keusgen
Fraunhofer Heinrich Hertz Institute
Berlin, Germany
michael.peter@hhi.fraunhofer.de

***Abstract*—In this paper, fundamental investigations of human shadowing at 60 GHz are presented. Different electromagnetic models are analyzed regarding their accuracy and computional effort. Therefore, different geometrical representations of the human body, namely circular cylinders with different dielectric properties, the dielectric elliptic cylinder, and the so-called multiple knife edge (MKE) model are investigated. Based on these models, the influence of the object shape on the modeling accuracy and the necessity of taking into account the human skin or clothing are estimated. In addition, a comparison of Doppler spectra based on measurements and UTD simulations is presented.**

I. Introduction

Currently, the standardization activities IEEE802.15.3c, IEEE802.11ad and ECMA387 as well as the industrial consortia WirelessHD and the WiGig alliance are aiming at specifications of short range wireless multi-Gbps systems. All five groups focus on the 60 GHz frequency band, which offers up to 9 GHz of unlicensed bandwidth capable of enabling the intended multi-Gbps data rates. In order to evaluate the system performance already during the specification, appropriate 60 GHz channel impulse response models are obligatory. Such models are often derived from ray tracing (RT) simulations (see e.g. [1], [2]). As human shadowing is a severe problem for wireless indoor mm-wave communications, it has to be taken into account in radio channel models [3]–[6]. Different models have been proposed for this purpose, including cylinders, knife edges or cuboids [4]–[9]. In this paper, such models are compared in order to judge for their applicability to be combined with RT. In addition to the shadowing, human activity may also lead to a Doppler shift due to time-varying multipath components (MPC) that are diffracted or reflected at moving bodies (see e.g. [2]). This effect will be analyzed by comparing time-variant channel measurements and simulations. The paper is structured as follows. The comparison between chosen human blockage models will be given in section II. In section III, the investigations that are related to the Doppler effect are presented. Section IV concludes the paper.

II. Comparison of 60 GHz Human Blockage Models

Three different geometric models representing the human body have been considered. The list below summarizes the considered theories:

1) *Circular cylinder*
   a) *Perfectly conducting (PEC) cylinder,* UTD approximation [10].
   b) *Dielectric cylinder*, taking into account the permittivity of the human skin [11].
   c) *Dielectric-coated perfectly conducting cylinder*, taking into account clothing [12].
2) *Dielectric elliptic cylinder* as a better geometric representation of the human body [13].
3) *Multiple knife edge diffraction (MKE)*, a simple, computationally inextensive model [6].

In the following, the presented models are analyzed regarding their suitability for the modeling of human blockage at 60 GHz. The focus here lies on three main requirements:

1) The model should accurately reproduce the empirically observed human shadowing characteristics.
2) As the model is likely to be used in extensive simulations to generate data sets for the development of statistical models, the computational effort must be manageable.
3) It should be easy to integrate the model into ray tracing simulations.

Regarding the third requirement, a ray-based theory would be most suitable. Among the analyzed theories, only the UTD is ray-based and hence most appropriate. In contrast to the other methods, its results contain information about ToA, AoA and AoD of the different involved field components. Nevertheless, approximations for these parameters can be derived for all models. Regarding the computational effort, the MKE model is more efficient than any other model, followed by the UTD. The exact solutions rely on sums of Bessel functions and are 200 to 70,000 times slower than the MKE approach.

The correct reproduction of the shadowing attenuation will be discussed in detail in the following. At first the influence of the human skin, the object shape and the influence of clothing is analyzed. Then, the models are compared with measurements in order to judge the accuracy.

1) Influence of the human skin: The circular cylinder has been used to model human blockage at 60 GHz before [9]. In this paper, we will discuss whether a cylinder with the dielectric properties of human skin is a better assumption than the PEC cylinder. Therefore, the scattering of a plane wave is compared for both cases. A variety of simulated and measured electrical properties of the skin at 60 GHz is available. Here, a relative permittivity of $\varepsilon_d = 8.05 - j4.13$ has been adopted for the human skin [14]. Please note that the influence of clothing will be analyzed separately subsequently in this section.

Fig. 1a shows the loss for the dielectric cylinder in relation

978-88-907018-3-2/13 ©2013 IEEE

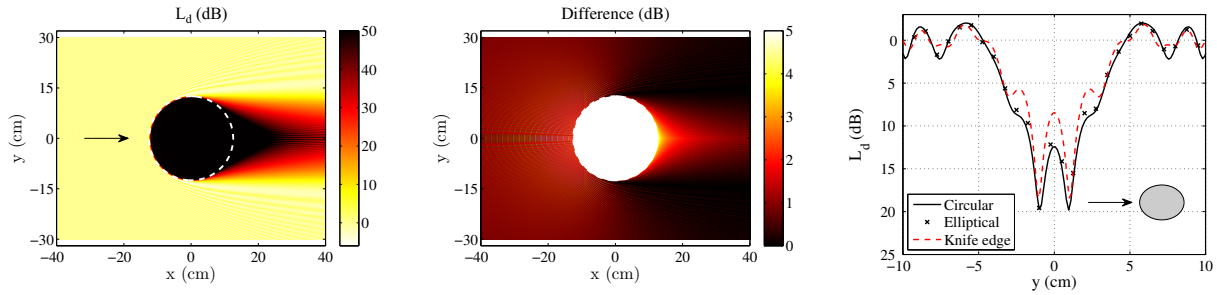

(a) Shadowing loss of a dielectric (skin) cylinder.

(b) Difference between loss for PEC and dielectric (skin) cylinder

(c) Modeled shadowing behind the human arm.

Figure 1: Simulated shadowing characteristic for the human body and the human arm, respectively.

to the case without cylinder, which would be the lossless propagation of a z-polarized plane wave in x-direction. The loss is shown in the $z = 0$ plane. The cylinder diameter is chosen to be 25 cm according to the typical width of the human body. Directly behind the cylinder obstacle in the deep shadow region, very high losses occur, whereas the diffracted power increases at larger distances. In front of the cylinder, fading can be observed due to the interference between scattered and incident field. These fading characteristics are more pronounced with higher maxima and lower minima for the PEC cylinder as here the reflectivity is higher than for the dielectric cylinder. In Fig. 1b, the absolute difference between the loss distributions in the $z = 0$ plane is depicted. Directly behind the cylinder, the loss is up to 5 dB lower for the dielectric (skin) cylinder. However, it is noteworthy that in 90 % of the whole area the loss differs by at maximum 1 dB only. The area within the human body is not relevant for the envisaged application in channel models. Nevertheless, it is noteworthy that a meaningful comparison is not possible within the object as in the PEC case the electrical field vanishes.

2) Influence of object shape: The influence of the object shape is compared for the human arm. This is done because models for the extremities can help improving the modeling accuracy [5]. Apart from the extremities, the elliptic cylinder is also a better physical representation of the whole human body compared to the circular cylinder, as it approximates the cross section of the human torso more appropriately. Nevertheless, the investigation for the human torso is left out here for the sake of briefness. In order to model the human arm, the minor and the major radius of the elliptic cylinder are chosen to be 2.75 and 3.5 cm, which are typical values. A plane wave propagates along the major axis of the elliptic cross section (see Fig. 1c). In addition to the elliptical cylinder model, the results for the circular cylinder and the MKE are shown. The cylinder diameter as well as the dimensions of the MKE are chosen equivalent to the relevant axes of the elliptical cylinder. This comparison is done for the shadow region 0.2 m behind the cylinder and the transition to the lit region. In both cases, almost no difference between circular and elliptical cylinder model is visible. Regarding the MKE solution, the interference maxima are higher and the characteristic in the lit region also slightly deviates from the other two models. The same behavior could be observed for the wave propagating along the minor axis of the body. Of course, one big disadvantage of the circular cylinder model is, that it does not account for the different dimensions of length and width of the arm cross section.

3) Influence of clothing: In order to analyze the influence of clothing further, additional measurements of a brass cylinder have been performed. These measurements have been carried out at a single frequency of 69 GHz using the measurement setup described in [15]. A cylinder with a radius of 4 cm has been measured barely and covered with 5 mm of cotton. The results presented above have shown that the human skin can be assumed to be a PEC because no significant difference could be observed. Hence, the covered metallic cylinder is a sufficient approximation for clothing on skin. Fig. 2a depicts the angular dependent results for vertical (VV) and horizontal (HH) polarization. The negative angles corresponds to the shadowing region. In the metallic case, the characteristic is steeper and the absolute loss is higher for the vertical polarization compared to horizontal polarization, which is expected. Interestingly, in case of vertically polarized waves, the clothing leads to losses, *higher* by up to 20 dB in the shadowing region. This does not hold for the horizontal polarization. Here, the maximum difference amounts to only 6.9 dB, however, mostly the metal cylinder case shows the lower losses. It is noteworthy that the diffraction behavior is highly sensitive to the layer thickness and the dielectric properties of the clothing. This will also be analyzed in the next section.

4) Validation by measurements: In order to validate the human blockage models, simulation results have been compared with human blockage measurements from [3]. Up to this point, the mere amplitude of individual shadowing events has been considered. However, measurements have revealed that the phase of a signal changes rapidly during an event. This is especially important for the modeling of time-variant channel impulse responses. Fig. 2b illustrates an exemplary measured shadowing event and the corresponding MKE simulation results. The figure shows the amplitude as well as the phase. The amplitude characteristic is only shown as a reference, here, because it has been thouroughly discussed in our previous work [3], [4]. The shadowing event is almost symmetrical. The phase stays nearly constant up to the instant of time,

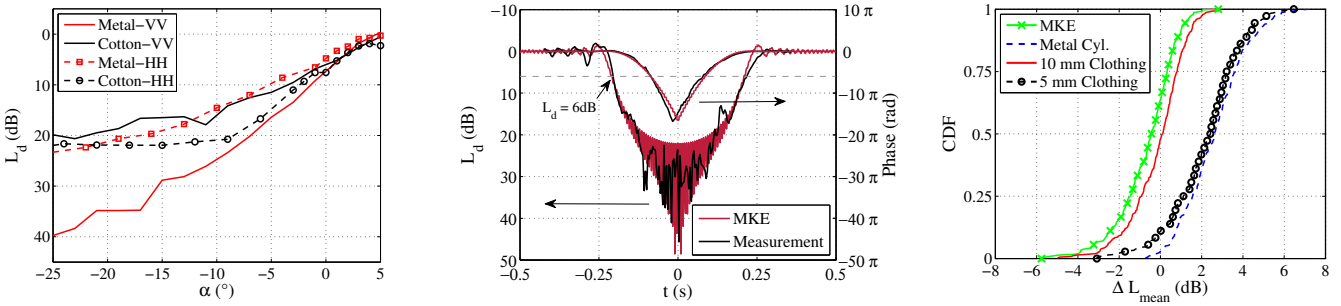

(a) Influence of clothing.

(b) Exemplary shadowing event.

(c) CDF of differences between averaged measured and simulated shadowing loss.

Figure 2: Comparison of human blockage theories and measurements.

when the loss reaches 6 dB. This corresponds to the position where the person just shadows the LOS connection. Before this point, the loss characteristic is dominated by the LOS link, which has a constant phase. In the shadow region behind this point, the diffracted components dominate. Compared to the small wavelength, these components change their length and hence the phase very fast. The phase decreases by $16\,\pi$ in the first half of the event and increases afterwards. This can be explained by the fact that the component diffracted around the front of the body, which gets longer with time, dominates first. Then, in the second half of the event, the component diffracted at the back dominates, which gets shorter with time. Despite a small time shift, which could be caused by a varying walking speed in the measurements, the agreement of the measured and the simulated phase is very good.

Besides this qualitative comparison, a quantitative comparison in terms of the fading statistics is carried out for a person walking through the direct path between transmitter and receiver. The underlying measurements have been performed with a 60 GHz real time wideband 2x2 MIMO channel sounder. At this point, the sole LOS MPC is considered. A detailed description of the measurement setup as well as a comparison between measurements, UTD and MKE, can be found in [4]. In the present paper, the comparison has been carried out for the MKE model, the PEC cylinder (UTD) and the coated cylinder. The UTD and the MKE model have been chosen because of their low computional effort as well as due to the fact that the previous analysis has shown that assuming a PEC instead of human skin is sufficient. In order to study the impact of clothes, the coated cylinder model is also considered here. Two different cases have been simulated. A 5 mm and a 10 mm thick dielectric coating is assumed to emulate a fleece layer with $\epsilon_d = 1.25 - j0.042$ [14]. Fig. 2c shows the CDFs of the differences between measured and simulated shadowing loss. In principle, all models show a good agreement with the experimentally observed shadowing events. The focus here lies on the deep shadowing region. For this reason, the mean value of the attenuation higher than 10 dB has been taken into account for every shadowing event. The averaging is done as already slight temporal displacements between measured and simulated interference patterns would lead to very high differences. Altogether, the CDF is derived from 360 different shadowing events with distances between RX and TX ranging from 2 to 10 meters. The CDFs reflect the behavior already observed in Fig. 2b. The PEC cylinder model tends to overestimate the attenuation by up to 6 dB, whereas the MKE and the coated cylinder model (10 mm coating) in principle show better performance with average deviations of 0.1 and 0.4 dB, respectively. In case of the MKE model, this is quite surprising as the PEC cylinder definitely provides a better approximation of the human body than knife edges. In case of the coated cylinder it is also an interesting result, that obviously the consideration of clothing can lead to a significantly higher model accuracy. Nevertheless, the accuracy is very sensitive to the coating parameters, i.e. thickness and dielectric properties. The modeling error for the 5 mm coating is, for example, almost as high as for the bare PEC cylinder. The dielectric properties as well as the layer thickness of the clothing, which have been worn during the measurements, are not known. Nevertheless, the results suggest that it is possible to enhance the modeling accuracy by taking into account clothing.

III. Doppler Effect

Even in application scenarios with nomadic devices, human activity may lead to a Doppler shift due to time varying multipath components diffracted or reflected at moving persons. The Doppler effect at mm-wave frequencies has already been treated in literature (see e.g. [2]). Nevertheless, a direct comparison between measurement results and simulations cannot be found and is presented here for the first time. In order to estimate the expected Doppler shift, a scenario is

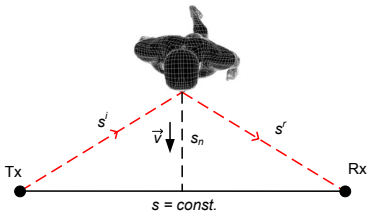

Figure 3: Geometry for the calculation of the Doppler shift.

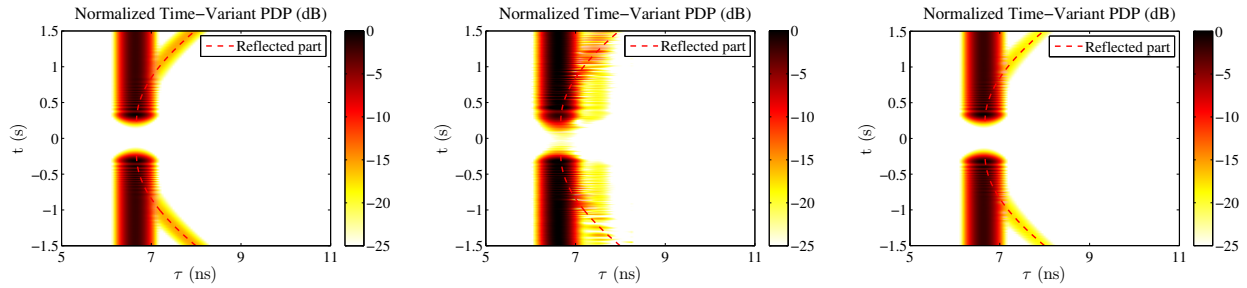

(a) Cylinder UTD, omni antennas. **(b)** Measurement, omni antennas. **(c)** Cylinder UTD, horn antennas.

Figure 4: Time-variant PDPs based on broadband measurements and simulations.

examined here, where a person crosses the LOS link perpendicularly with walking speed v. The investigation is based on narrowband [3] as well as broadband measurements [4], [16]. A schematic with all required geometrical parameters describing the scenario is shown in Fig. 3. In this symmetrical example, the ToA of the multipath component reflected at the front of the person can be derived by its length s^{r+i} taking into account the geometry:

$$s^{r+i}(t) = 2\sqrt{(v \cdot t)^2 + \left(\frac{s}{2}\right)^2} \tag{1}$$

The ToA of the reflection at the back, after the person has passed the ray is determined analogously. Please note that Eq. (1) is only valid before and after the actual shadowing event. Additionally, the term $v \cdot t$ has to be corrected by the body width, which is omitted in the equation to support ease of reading. In our analysis, $t = 0$ is defined in the middle of the shadowing event. Figs. 4a and 4b depict power delay profiles from a simulation according to the UTD together with time-variant measurements. In the measurements quasi omnidirectional antennas have been used. Additionally, the ToA characteristics expected according to Eq. (1) are shown as a dashed line. Both, simulations and measurements, have been performed for a 3-GHz-wide band around a center frequency of 60 GHz [4], [16]. In a post-processing a Kaiser window has been applied in frequency domain. Afterwards, the results have been transformed to the time domain via IFFT. Please note that this post-processing causes the pulse broadening over τ, which can be observed in Figs. 4a and 4b. The simulated power delay profile agrees quite well with the measured one. In both PDPs, the LOS component as well as the hyperbolic characteristic of the MPC reflected at the body is visible. Close to the actual shadowing event both components interefere, leading to fluctuations of the amplitude. It is noteworthy that the MPCs diffracted around the body are expected close to $t = 0$, but could not be resolved in the measurements due to the limited temporal measurement resolution. In addition, Fig. 4c illustrates the supression of the reflected MPC by directive antennas. There, Gaussian beam patterns [1] with half power beamwidths of 20° have been used in the UTD simulations. This will be analyzed in detail below together with the discussion of the Doppler shift.

The Doppler shift of the reflected MPC depends on the change of length of s^{r+i}. In the presented scenario, the time-variant Doppler shift is calculated by:

$$\nu_{Doppler}(t) = -\frac{2v^2 t f_c}{c\sqrt{(v \cdot t)^2 + \left(\frac{s}{2}\right)^2}}. \tag{2}$$

It is noteworthy that in indoor environments, more complex scenarios appear. On the one hand, different MPCs will have different Doppler shifts. On the other hand, higher Doppler shifts can occur in case of multiple reflections at the human body and additional objects like walls or furniture. In addition, the movement of different persons relative to each other will also lead to higher Doppler shifts. As higher order MPCs simultaneously exhibit higher losses, nevertheless, the given case of a person crossing the direct path between TX and RX will definitely have the highest impact. The evaluation above is only valid in LOS situations. However, in the shadow region, the Doppler shift is induced by the change in length of the diffracted rays around the body. Here, the analytical derivation of the Doppler shift is not possible as the geometrical parameters for the UTD are determined numerically [10].

Fig. 5a depicts the time-varying Doppler spectrum derived from simulations assuming omnidirectional antennas. The Doppler spectrum $P_B(\nu_{Doppler})$ is calculated as the Fourier transform of the time correlation function $R_H(\Delta t)$ of the time variant transfer function $H(t)$ [17]. For the calculation of $R_H(\Delta t)$, a time window of 66 ms has been used corresponding to a distance of about $10\,\lambda$ in order to fulfill the assumption of wide-sense stationarity. In addition, a Hamming window has been applied before the Fourier transform. For the UTD, a cylinder radius of 19 cm and a walking speed of $v = 0.75\,\frac{\mathrm{m}}{\mathrm{s}}$ have been assumed. TX and RX have been separated by 2.63 m. Here, narrowband measurements at a frequency of 67 GHz form the basis for the investigations [3]. According to Eq. (2), a maximum Doppler shift of 335 Hz is expected. It is noteworthy that due to the limited temporal resolution components of the Doppler spectrum will be slightly broadened. In the figure, a strong Doppler component is observed for $\nu_{Doppler} = 0$ coming from the time-invariant LOS component. Only in the shadowing area around $t = 0$, this component slightly changes to values of a few ten Hz. This behavior is caused by the change in length of the diffracted rays around the body mentioned above. The reflected MPC

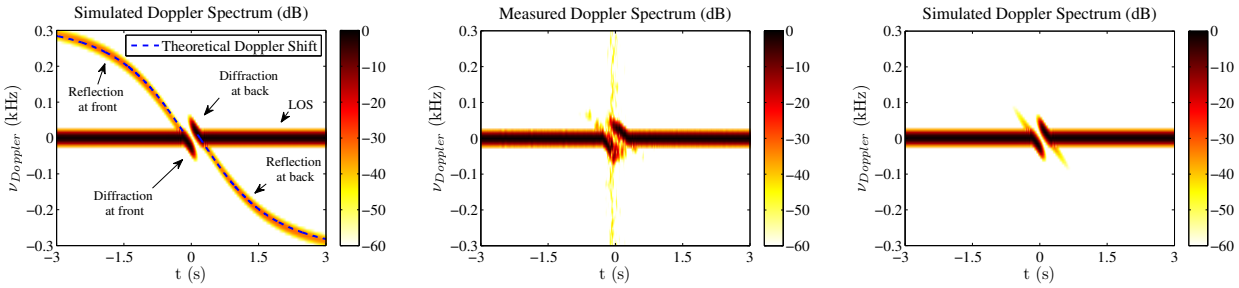

(a) Cylinder UTD, omni antennas. **(b)** Measurement, horn antennas. **(c)** Cylinder UTD, horn antennas.

Figure 5: Time-variant PDPs based on narrowband measurements and simulations.

causes a Doppler shift that decreases with time according to Eq. (2). As expected, the function tends to converge to the value of 335 Hz. In the corresponding measurements (Fig. 5b), this component disappears very fast, when the person moves away from the LOS link. The explanation for this is that here directive horn antennas have been used suppressing the reflected MPC (c.f. Fig. 4c). Accordingly, the antennas also suppress components in the Doppler spectrum. For the sake of completeness, Fig. 5c shows the UTD simulation results employing the Gaussian beam patterns. As expected, in this case, the simulations agree very well with the measurements.

IV. Conclusion

In this paper, different cylindrical structures as well as the MKE have been analyzed with respect to the geometrical modeling of the human body. Based on these theories, the suitability of the approaches for deterministic radio channel modeling has been investigated. It could be shown that it is not necessary to consider the dielectric properties of the human skin, as its conductivity is high enough to be assumed as a perfect electrical conductor instead of a dielectric material for the envisaged application. Regarding the model geometry, it has been pointed out that there are no significant deviations between elliptical and circular cylinders. Finally, the model results have been validated with measurements, which has lead to two interesting results. The agreement between the knife edge diffraction simulations and the human blockage measurements is quite good. Hence, the MKE approach has been used together with ray tracing for the development of stochastic channel models [6], [16]. In addition, clothing can have a significant influence on the attenuation under certain circumstances. Compared to the measurements, the cylinder model accuracy could be increased by more than 2 dB taking into account clothing. On the other hand, this model is very sensitive to the thickness and the material of the clothing.

In addition, the Doppler shift due to human activity has been investigated. Time-variant Doppler spectra have been derived from simulations as well as channel measurements. Their comparison reveals that it is possible to reproduce the Doppler behavior at 60 GHz with the cylinder UTD. The measurement results also approves that directive antennas suppress the influence of the Doppler spread on the system performance.

References

[1] A. Maltsev et al., "Channel Models for 60 GHz WLAN Systems, doc.: IEEE 802.11-09/0334r8," *https://mentor.ieee.org/802.11/documents*, 2010.

[2] P. Smulders, "Statistical Characterization of 60-GHz Indoor Radio Channels," *IEEE Transactions on Antennas and Propagation*, vol. 57, no. 10, pp. 2820 –2829, oct. 2009.

[3] M. Jacob, C. Mbianke, and T. Kürner, "A Dynamic 60 GHz Radio Channel Model for System Level Simulations with MAC Protocols for IEEE 802.11 ad," in *14th IEEE ISCE Conference*, 2010.

[4] M. Peter, M. Wisotzki, M. Raceala-Motoc, W. Keusgen, R. Felbecker, M. Jacob, S. Priebe, and T. Kürner, "Analyzing Human Body Shadowing at 60 GHz: Systematic Wideband MIMO Measurements and Modeling Approaches," *EuCAP, Prague, Czech Republique*, 2012.

[5] C. Gustafson and F. Tufvesson, "Characterization of 60 GHz Shadowing by Human Bodies and Simple Phantoms," in *EuCAP, Prague, Czech Republique*. IEEE, 2012, pp. 473–477.

[6] M. Jacob, S. Priebe, A. Maltsev, A. Lomayev, V. Erceg, and T. Kürner, "A Ray Tracing Based Stochastic Human Blockage Model for the IEEE 802.11ad 60 GHz Channel Model," *EuCAP, Rome, Italy*, pp. 1–5, 2011.

[7] M. Ghaddar, L. Talbi, T. Denidni, and A. Sebak, "A conducting cylinder for modeling human body presence in indoor propagation channel," *IEEE Transactions on Antennas and Propagation*, vol. 55, no. 11, pp. 3099 –3103, nov. 2007.

[8] J. Kunisch and J. Pamp, "Ultra-wideband double vertical knife-edge model for obstruction of a ray by a person," in *ICUWB 2008*, vol. 2, 2008, pp. 17–20.

[9] A. Khafaji, R. Saadane, J. El Abbadi, and M. Belkasmi, "Ray Tracing Technique based 60 GHz Band Propagation Modelling and Influence of People Shadowing," *International Journal of Electrical, Computer, and Systems Engineering*, vol. 2, no. 2, pp. 102–108, 2008.

[10] P. Pathak, W. Burnside, and R. Marhefka, "A Uniform GTD Analysis of the Diffraction of Electromagnetic Waves by a Smooth Convex Surface," *IEEE Transactions on Antennas and Propagation*, vol. 28, no. 5, pp. 631–642, 1980.

[11] C. A. Balanis, *Advanced Engineering Electromagnetics*. Wiley, 1989.

[12] C. Tang, "Backscattering from Dielectric-Coated Infinite Cylindrical Obstacles," *Journal of Appl. Physics*, vol. 28, no. 5, pp. 628–633, 1957.

[13] J. Stratton, *Electromagnetic Theory*. McGraw-Hill New York, 1941.

[14] M. Zhadobov, N. Chahat, R. Sauleau, C. Le Quement, and Y. Le Drean, "Millimeter-Wave Interactions with the Human Body: State of Knowledge and Recent Advances," *International Journal of Microwave and Wireless Technologies*, vol. 3, no. 02, pp. 237–247, 2011.

[15] M. Jacob, S. Priebe, R. Dickhoff, T. Kleine-Ostmann, T. Schrader, and T. Kürner, "Diffraction in mm and sub-mm Wave Indoor Propagation Channels," *IEEE Transactions on Microwave Theory and Techniques*, vol. 60, no. 3, pp. 833–844, 2012.

[16] M. Jacob, S. Priebe, S. Rey, M. Peter, M. Wisotzki, W. Keusgen, R. Felbecker, and T. Kürner, "Extension and Validation of the IEEE 802.11ad 60 GHz Human Blockage Model," *EuCAP, Gothenburg, Sweden*, 2013.

[17] A. Molisch, *Wireless Communications*. New York: Wiley, 2005.